https://doi.org/10.5194/cp-2023-11
Preprint. Discussion started: 20 March 2023

Climate of the Past Discussions

Contribution of Lakes in Sustaining Greening of the Sahara during the Mid-Holocene

Yuheng Li[1], Kanon Kino[1], Alexandre Cauquoin[2] and Taikan Oki[1]

[1]Department of Civil Engineering, Graduate School of Engineering, the University of Tokyo, Tokyo, Japan.
[2]Institute of Industrial Science, The University of Tokyo, Kashiwa, Japan.

Correspondence to: Yuheng Li (yuheng@rainbow.iis.u-tokyo.ac.jp)

Abstract. The contribution of lake-climate feedback to sustain the Green Sahara in the mid-Holocene (MH, 6000 years ago) is still under debate. To assess the lake-induced climate response over North Africa, we investigated the roles of Western Sahara lakes and Megalake Chad using reconstructions of MH Sahara lake maps as surface boundary conditions for the isotope-enabled atmospheric model MIROC5-iso. Our results show that the Western Sahara lakes pushed the West African monsoon northward and extended it eastward by expanding Megalake Chad. Such lake-climate feedback was caused by the cyclonic circulation response related to weakened African Easterly Jet and enhanced Tropical Easterly Jet. According to Budyko aridity index, the northwestern Sahara climate region shifted from hyper-arid to arid or semi-arid with lake expansion. Moreover, precipitation scarcity could be reduced by up to 13% to sustain semi-humid conditions. Such lake-climate feedback alleviates the Sahara aridity but relies on lake positions in the monsoon regions. Our findings are promising for understanding the contribution of lakes to sustaining the Green Sahara.

https://doi.org/10.5194/cp-2023-11
Preprint. Discussion started: 20 March 2023

Climate of the Past Discussions

1 Introduction

Much paleoclimate evidence shows that in the mid-Holocene (MH, 6000 years ago), the Sahara Desert, the largest hot desert in the world, was much wetter and greener compared with the present-day climate (Claussen, M. et al., 2017). This period, called Green Sahara (GS) or African Humid Period (AHP), was mainly caused by the Earth's orbital cycle revolution on obliquity, eccentricity, and precession, leading to high seasonality insolation in the Northern Hemisphere (Otto-Bliesner et al., 2017) with approximately 7% higher summer insolation over North Africa (NAf) during the MH than today (Berger, 1988). Under such orbital forcing changes, the West African Monsoon (WAM) strengthened and extended northward, leading to distinct rainfall regimes and increased vegetation along with narrow desert zones in Sahara (Kutzbach et al., 2020). Although the GS climate is highly correlated with orbital forcing, state-of-the-art general circulation models (GCMs) cannot account for the widespread precipitation during the GS period (Braconnot et al., 2007; Perez-Sanz et al., 2014; Harrison et al., 2015; Brierley et al., 2020). Hence, researchers have investigated oceanic and terrestrial roles in sustaining the GS. Remote oceanic feedback contributes to enhanced summer monsoon with increasing sea surface temperature (Braconnot et al., 1999; Kutzbach & Liu, 1997; Zhao et al., 2005) and winter rainfall (Cheddadi et al., 2021) over NAf. Further, inland terrestrial system is affected by vegetation growth (Thompson et al., 2022), especially interactions with soil (Kutzbach et al., 1996; Chen et al., 2020), dust reductions (Messori et al., 2018), and dust-cloud interactions (Hopcroft & Valdes, 2019; Braconnot et al., 2021). Despite terrestrial and ocean improvements in the model modules and an understanding of their roles in the GS climate, the MH climate simulations from the Paleoclimate Modeling Intercomparison Project 4 (PMIP4) still underestimate the northward WAM extension (Brierley et al., 2020).

Despite implementing all terrestrial feedback in model MH simulations, biases still exist in the contribution of open-water surfaces (lakes and wetlands) over NAf that are often set as the same as in pre-industrial control simulations. Hoelzmann et al. (1998) reconstructed the Megalake Chad distribution in the Sahara during the Holocene (hereinafter small-lake map; MH_98 in Tables 1 and S1). By adopting this small-lake map to the Community Climate Model version 3 (CCM3) climate model, Broström et al. (1998) and Carrington et al. (2001) found that Megalake Chad produced more localized hydrological changes and did not contribute to the northward WAM movement. Contrastingly, using an improved atmospheric GCM (AGCM), Krinner et al. (2012) further suggested that the open-water surface effect was underestimated in previous studies that reported the northward WAM shift, with as a consequence a doubling of the regional precipitation rates. However, the disadvantage of MH_98 is that it does not include any other MH Megalakes beyond Megalake Chad (Holmes & Hoelzmann, 2017). Hence, Chandan and Peltier (2020) further added dedicated MH Megalakes to the small-lake map and investigated the lake effect using a fully coupled atmosphere-ocean GCM (AOGCM). They reported that the increase in precipitation from the lakes was weak, and the lake location did not considerably influence precipitation. Hence, the role of Megalake Chad in contributing to the humidification of the Sahara is still under discussion. Furthermore, the lakes in the western

https://doi.org/10.5194/cp-2023-11
Preprint. Discussion started: 20 March 2023


Climate of the Past Discussions

Sahara also potentially contribute to WAM. Tegen et al. (2002) further indicated the presence of larger lakes and wetlands over the western Sahara based on dust emission simulations (hereinafter potential maximum-lake map; MH_02 in Tables 1 and S1). Based on the MH_98 and MH_02 lake maps, Specht et al. (2022) investigated the impacts of the latitudinal position of lakes and wetlands on changes in precipitation, and initially highlighted the influence of western lakes on the northward WAM shift. These studies suggested that western lakes and Megalake Chad may play different roles in humidifying the Sahara, and this aspect requires further investigation.

The above-mentioned studies on lake-climate feedback also explored the underlying physical mechanisms by which lake thermal and dynamic forcing affects the atmospheric circulation of the African monsoon system. For example, compared with the enhanced localized water cycling forced by lake evaporation (Broström et al., 1998; Carrington et al., 2001), Krinner et al. (2012) considered that the cooling effect that stabilizes convection is only locally applicable to deep lakes but increases the predictable water in summer and delays cooling in autumn, thereby extending monsoon. Using the latest information on the NAf monsoon system, the contribution of the Sahara Heat Low (SHL) and Sahara Highs in western Sahara, the African Easterly Jet (AEJ) in the middle atmosphere (600 hPa), and Tropical Easterly Jet (TEJ) in the upper atmosphere (200 hPa) on the near-surface westerly flow northward and rainfall has been further discussed (Biasutti & Sobel, 2009; Claussen et al., 2017; Kuete et al., 2022). Chandan and Peltier (2020) further stressed that such a cooling effect could weaken the SHL and local convection, reducing the precipitation. On the contrary, Specht et al. (2022) found that a weakened AEJ enhanced inland moisture transportation, leading to a northward and prolonged rain belt. Owing to these discrepancies, the mechanisms of lake-climate interaction in the NAf monsoon system remain unclear.

To address these issues, the present study assessed the contribution of Western Sahara lakes and Megalake Chad in humidifying the Sahara region during the MH using the isotope-enabled AGCM MIROC5-iso (Okazaki & Yoshimura, 2019). To consider the large uncertainty in MH lake reconstructions (Quade et al., 2018), sensitivity experiments have been conducted with the original two sets of lake reconstructions (Hoelzmann et al., 1998; Tegen et al., 2002) and the recently-updated high-resolution lake reconstructions maps (Chen et al., 2021) over the NA during the MH. We discuss the influence of Western Sahara lakes and Megalake Chad on the WAM movement and the potential lake-climate mechanisms involved to sustain the Green Sahara.

2 Materials and Methods

2.1 Experiments and settings

We used the isotope-enabled version of the Model for Interdisciplinary Research on Climate version 5 (MIROC5, Watanabe et al., 2010), called hereafter MIROC5-iso (Okazaki and Yoshimura, 2019). MIROC5-iso adopts a three-dimensional primitive equation in the hybrid σ–p coordinate system. The resolution of MIROC5-iso was set to a horizontal spectral truncation of T42 (~280 km) and 40 vertical layers with coordinates. The parameterization schemes have been comprehensively described by Watanabe et al. (2010), Okazaki and Yoshimura (2019), and Kino et al. (2021).

https://doi.org/10.5194/cp-2023-11
Preprint. Discussion started: 20 March 2023

Climate of the Past Discussions

To assess the hydroclimatic influence of changes in the presence of lakes in NAf (0°–35° N; 20° W–40° E), we performed two control simulations as reference for the pre-industrial (year 1850, PI_{ref}) and MH (MH_{ref}) period and six MH sensitivity experiments (see Table 1). For every experiment, orbital forcing and greenhouse gas concentrations were set according to the PMIP4 protocol (Otto-Bliesner et al., 2017). Land surface boundary conditions (such as land-sea mask, ice sheets, soils, vegetation, and lakes) were set according to the Coupled Model Intercomparison Project Phase 5 (CMIP5) protocol for MIROC5 (Watanabe et al., 2010). Specifically, the Earth Topography five-minute grid (ETOPO5, https://www.ngdc.noaa.gov/mgg/global/etopo5.HTML) was used as global lake map boundary conditions for the control simulations. Each experiment was run for 60 years, and only the last 30 years were used for our analyses to get the soil moisture (SM) of the study at an equilibrium state, indicating a balanced land surface water budget. We used sea surface temperature, sea ice concentration, and water isotope content of the sea surface provided MPI-ESM-wiso PI and MH simulations (Cauquoin et al., 2019) as boundary conditions for MIROC5-iso. Figure S1a shows the global lake distribution used for MH_{ref} and PIref experiments using ETOPO5 as in MIROC5 standard simulations. We found that few lakes existed in NAf (Figure S1b). In our six sensitivity MH experiments, only the lake map was changed in NAf, while other boundary conditions were kept the same as in MH_{ref} (Table 1).

Table 1. Experiments Setting

Experiment	GHG + Orb	Sea Surface	Lakes in the North Africa
PI_{ref}	PI*1	PI*2	ETOPO5*3
MH_{ref}	MH*1	MH*2	
MH_{C}			MH_98*4
MH_{WC}			MH_02*4
MH_{WCE1}			MH1*4
MH_{WCE2}			MH2*4
MH_{WCE3}			MH3*4
MH_{WCE4}			MH4*4

*1 Following PMIP4 Protocol

*2 Cauquoin, Werner et al. (2019)

*3 National Geophysical Data Center, 1993. 5-minute Gridded Global Relief Data (ETOPO5) National Geophysical Data Center, NOAA. Doi:10.7289/V5D798BF.

*4 The details of the lake reconstructions can be seen in Table S1.

The reconstructed lake maps in NAf used for our sensitivity experiments are summarized in Table S1 and are shown in figure S2. MH_{C} uses the MH_98 lake maps (Hoeltzmann et al., 1998), with only the Megalake Chad, over 15°–20° E and

https://doi.org/10.5194/cp-2023-11
Preprint. Discussion started: 20 March 2023

Climate of the Past Discussions

10°–20° N (Figure S2a). The MH_{WC} experiment uses the MH_02 lake maps (Tegen et al., 2002) with more numerous western and northern lake areas over 0°–10° W and 10°–20° N in addition to Megalake Chad (Figure S2b). The MH_{WCE1}–MH_{WCE4} experiments use the MH1-4 lake maps from Chen et al. (2021). They show an increasing lake fraction in Megalake Chad and eastern lakes in South Sudan around 0–20° N, with a gradually increasing scattered west lake area (Figure S2c–f) compared with the MH_98 and MH_02 lake maps. MH4 accounting for the largest lake proportion among the western and eastern lakes, and the Megalake Chad, is mainly different from the MH2 lake map for the latter (Figure S2d and S2f). The average main lake fraction over the NAf region according to these different reconstructions varies from 1-3 % compared with the present global land surface area (~1.48 × 108 km2) (Figure S2g). Generally, lakes and wetlands are persistently saturated or near-saturated areas that are regularly subjected to inundation or shallow water tables in the absence of human disturbances (Tootchi et al., 2019). In this study, wetlands are considered as lakes in our climate model.

We investigated the contribution of the Western Sahara lakes by comparing the MH_C and MH_{WC} experiments. The Megalake Chad influence on NAf climate was quantified using the MH_{WCE2} and MH_{WCE4} results. For evaluation of our model results, we compared the isotope outputs from MIROC5-iso with available observations from natural archives (e.g., δ18O in ice cores and speleothems) as in Cauquoin et al. (2019).

2.2 Climate model validation method

To evaluate our MH simulation, we used measured isotope datasets from ice cores and continental speleothems. We used 5 Greenland and 10 Antarctic ice cores, selected from the comprehensive compilations of Sundqvist, Kaufman et al. (2014), and WAIS Divide Project Members (Fudge, Steig et al., 2013). They are reported in Table 1 of Cauquoin et al. (2019). We also added to this dataset MH−PI δ18O anomalies measured from four (sub)tropical ice cores (Huascaran, Sajama, Illimani, and Guliaa ice cores), which are reported in Table 3 of Risi et al. (2010). Furthermore, we extracted 57 entities from the SISALv2 (Speleothem Isotope Synthesis and Analysis version 2) dataset (Comas-Bru et al., 2020 ESSD), for which averaged δ18O values of calcite or aragonite are available for both the MH and PI period. As recommended by Comas-Bru et al. (2019), we defined here PI and MH as the means of 1850-1990 CE and 6 ± 0.5 ka periods, respectively. The measured δ18O of calcite or aragonite are converted into δ18O of drip water using equations 1 or 2 of Comas-Bru et al. (2019), respectively, after conversion from V-PDB to V-SMOW scale (equation 3 of Comas-Bru et al. (2019)). The annual mean surface air temperature from MIROC5-iso is used for the conversion.

2.3 Analysis method

2.3.1 Hydroclimate analysis

We analyzed hydroclimate changes based on the ratio with the MH_{ref} results.

$$Ratio_{exp} = \frac{Exp - MH_{ref}}{MH_{ref}} \times 100\% , \quad (1)$$

https://doi.org/10.5194/cp-2023-11
Preprint. Discussion started: 20 March 2023


Climate of the Past Discussions

The water vapor flux was also calculated to explain the precipitation changes. The zonal component of the integrated flux (Fu) is:

$$F_u = \int_{300hpa}^{ps} \frac{uq}{g} dP \,, \quad (2)$$

where u is the horizontal wind, q the specific humidity, p the pressure at a given vertical level, g gravitational acceleration (9.8 m/s), and ps the surface pressure. The meridional component of the integrated flux (Fv) is expressed as:

$$F_v = \int_{300hpa}^{ps} \frac{vq}{g} dP \quad (3)$$

By combining Fu and Fv, the integrated vapor transport can be expressed as:

$$IVT = \sqrt{F_u^2 + F_v^2} \quad (4)$$

2.3.2 Budyko's aridity index

To assess climate zone transformation with the balance between available energy and water at the surface, Budyko's aridity index (Budyko & Miller, 1974) was calculated as a joint analysis using hydro-climatological variables as follows:

$$I = \frac{R_n}{lP} \quad (5)$$

where R_n is the net surface radiation, l the latent heat coefficient (2.5×10^6 J/kg), and P the precipitation at the surface. The change in the aridity index indicates regional shifts in hydroclimatic conditions.

3 Results

3.1 Model reproducibility

To evaluate the MH_{ref} results at global scale, we compared MH_{ref} - PI_{ref} with isotopic observations (Figure S3). We found a good model-data agreement, with a root mean square error and R-squared values of 0.81 ‰ and 0.33, respectively. Also, MIROC5-iso simulates a decrease in the isotopic composition of precipitation over NAf due to the enhanced monsoon during MH, in agreement with previous model studies (Schmidt et al., 2007; Risi et al., 2010; Cauquoin et al., 2019). Our simulation bias mainly originated from the ice cores in Antarctica and the speleothems in North America (Figure S3a). The isotopic performances in the PI_{ref} simulation were verified based on Okazaki and Yoshimura (2019) and Kino et al. (2021). Other previous studies also confirmed the general reproducibility of global MH experiments using the MIROC-series (O'Ishi & Abe-Ouchi, 2011; Ohgaito et al., 2021).

We further examined the model representation of WAM characteristics (Claussen et al., 2017). Based on the annual cycle of WAM (Thorncroft et al., 2011), we defined summer as June-July-August-September (JJAS) and winter as January-February-March (JFM). We focused on summer because of the large amount of precipitation caused by WAM. In both MH_{ref} and PI_{ref}, the Sahara Highs in the middle atmosphere were positioned at 20°–30° N and centered at 0° E (contours in Figures 1a and 1d). In the middle atmosphere, AEJ was found at 10°–15° N, corresponding to the precipitation belts (vectors and shaded

https://doi.org/10.5194/cp-2023-11
Preprint. Discussion started: 20 March 2023

areas in Figures 1a and 1d), and the concurrent TEJ at 0°–10° N in the upper atmosphere (vectors in Figures 1c and 1f). In the lower atmosphere (850 hPa), the SHL, centered in the hottest Sahara region at 10°–20° N (contours in Figures 1b and 1e), was associated with the monsoon westerly winds from the equatorial Atlantic Ocean to the continent (vectors in Figures 1b and 1e). While the monsoon westerly flow was at ~10° N in PI_{ref}, it moved to ~15° N in MH_{ref}. Given that the model bias and uncertainty in reproducing the AEJ still require improvement in reanalysis datasets (Kuete et al., 2022), our climate model efficiently captured the WAM patterns for investigating the sensitivity of WAM to lake expansions in the Sahara.

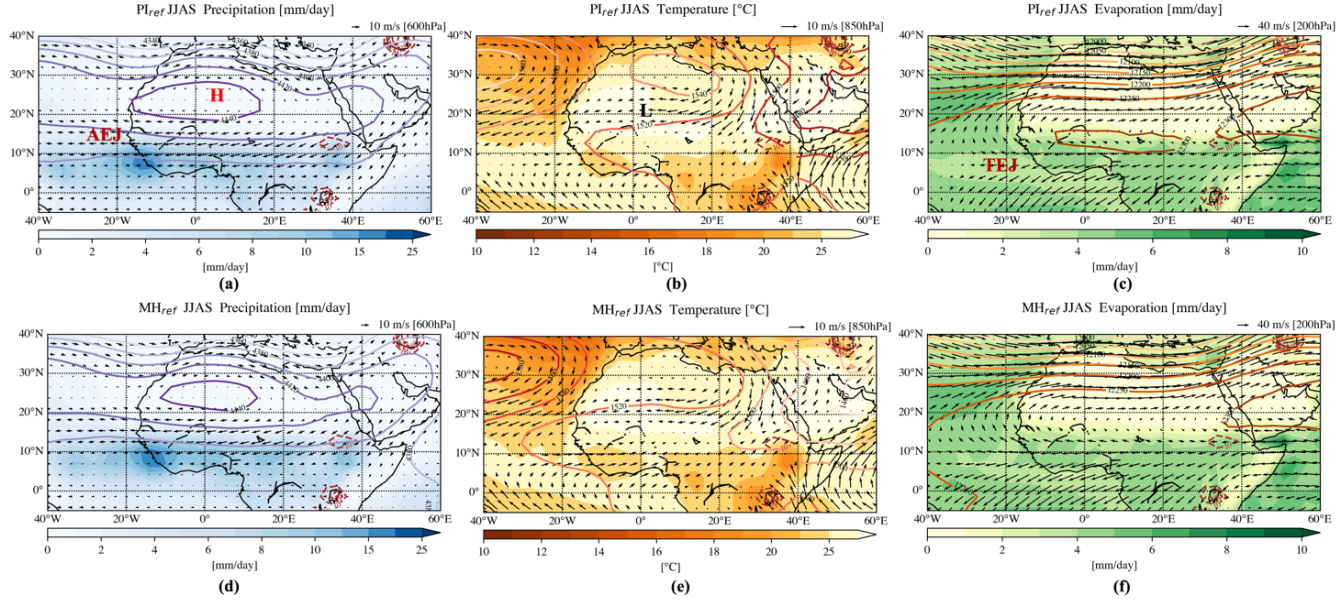

Figure 1: The simulated climatological precipitation and temperature responses for the Pre-industrial (PI) and mid-Holocene (MH) reference experiments on the summer season (June-July-August-September, JJAS). Subplot (a) is the precipitation with 600h Pa wind (arrow) geopotential high (counters). Subplot (b) is the surface temperature with 850h Pa wind (arrow) and geopotential high (counters). Subplots (c) and (d) are the same as (a) and (b), respectively, but for PI experiment. For (a-c), lake fraction [%] contours of the respective lake sensitivity experiment are shown with the red dashed lines, and the respective reference scale for the arrow is shown at the right top of each panel. The corresponding high pressure system, low pressure system, Africa Easterly Jet and Tropical Easterly Jet have been marked with 'H', 'L', 'AEJ' and 'TEJ'.

3.2 Hydroclimatic responses to the lakes in NAf

We investigated the influence of lake distribution in NAf on the hydroclimatic response by analyzing the differences between our lake sensitivity simulations and MH_{ref} for summer. First, we examined the influence of the Western Sahara lakes presence in addition to Megalake Chad. Without the Western Sahara lakes (MH_{C}), Megalake Chad marginally changed local precipitation and water transportation (shaded areas and vectors in Figure 2a). However, owing to the western lakes (MH_{WC}), the precipitation belt (originally at ~10° N in Figures 1a and 1d) strengthened, expanding northward and eastward to Megalake Chad (shaded areas in Figure 2b), and was associated with the enhanced anticlockwise water vapor transportation (vectors in Figure 2b). These findings suggested that the Western Sahara lakes enhanced the northward WAM extension. We further compared MH_{WCE2} and MH_{WCE4} experiments (Figures 2c and 2d) to MH_{ref} in order to assess the impact

https://doi.org/10.5194/cp-2023-11
Preprint. Discussion started: 20 March 2023

Climate of the Past Discussions
Open Access
EGU

of Megalake Chad size on the hydroclimatic influence of western lakes. We found that the western lakes at 10°–20° N could induce an enhanced precipitation belt with northwestward water transportation in the MH*WCE2* experiments (Figure 2c). With the expansion of Megalake Chad and eastern lakes, the precipitation belt extended eastward with a strengthened positive response (Figure 2d), suggesting the influence of Megalake Chad in eastward monsoon extension.

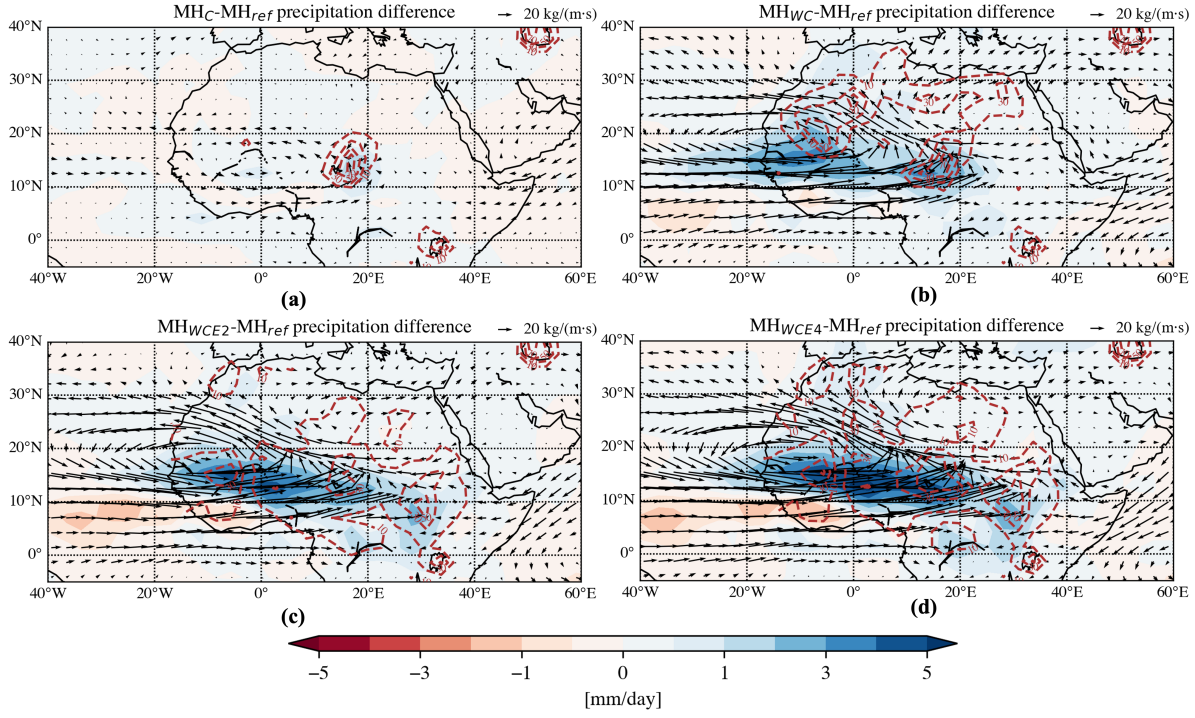

Figure 2: Anomalies relative to MH$_{ref}$ in simulated mid-Holocene climatological summer mean (June-July-August-September, JJAS) precipitation (shades) and integrated vapor transportation (IVT; arrows) for (a) MH$_C$, (b) MH$_{WC}$ and (c) MH$_{WCE2}$ and MH$_{WCE4}$ experiments, respectively. For (a)-(d), the lake fraction [%] contours of the respective lake sensitivity experiment are shown with the red dashed lines (contour spacing: 10%-30%-50%-70%-100%), and the respective reference scale for the arrow is shown at the right top of each panel.

Further, to investigate the mechanisms of the monsoon response to lake expansions, we analyzed the responses in land surface climate variables (SM, evaporation (Evap), and surface temperature (T2); shaded areas in Figure 3) and atmospheric circulations (geopotential height and horizontal winds; contours and vectors in Figure 3). In MH$_C$, Megalake Chad did not affect atmospheric circulations, but it affected the local hydrological cycle with slight increases in SM and Evap by 0.2 m and 2 mm/day, resulting in surface cooling around Megalake Chad by -0.4°C (Figure 3a, 3b, and 3c). In MH$_{WC}$, the western lakes induced similar local responses around the western lakes, with increased SM and evaporation flux accompanied by a surface cooling in northwest NAf, but with a stronger response than around Megalake Chad (Figure 3d, 3e, and 3f). The expansion of the western lakes impacts the atmospheric circulation, too. In the upper troposphere (200 hPa), TEJ was enhanced at 5°–15° N (vectors in Figure 3d). Further, the anticlockwise anomalies of horizontal winds in the middle atmosphere (vectors in Figure 3e), associated with the weakened Sahara High (contours in Figure 3e), suggested that the AEJ

https://doi.org/10.5194/cp-2023-11
Preprint. Discussion started: 20 March 2023

was weakened and shifted northward. In the lower atmosphere, the enhanced monsoon westerly flow at ~10°–20° N (vectors in Figure 3f) was associated with cyclone circulation over the Atlantic Ocean at ~20°–30° N, next to the weakened SHL (contours in Figure 3f).

Similar responses on hydroclimatic variables and atmospheric circulation were also found in MH$_{WCE2}$ and MH$_{WCE4}$ as in MH$_{WC}$. The increases in SM, Evap, and T2 extended more eastward in MH$_{WCE4}$ (Figure 3j, 3k, and 3l) compared with those in MH$_{WCE2}$ (shaded areas in Figure 3g, 3h, and 3i). The associated atmospheric circulation was further enhanced and extended eastward. Specifically, the TEJ became stronger, and Sahara High further weakened with stronger anticyclonic circulation anomalies extending eastward, leading to a weaker AEJ in MH$_{WCE4}$ than in MH$_{WCE2}$ (contours and vectors in Figure 3g, 3j 3h, and 3k). Moreover, the above cyclonic circulation in the lower atmosphere shifted southeastward at ~20° W, further extending the monsoon westerly flow eastward in MH$_{WCE4}$ compared with that in MH$_{WCE2}$ (contours and vectors in Figure 3i and 3l). Notably, owing to the southeastward extension of the cyclonic circulation response, the weak SHL signals in the MH$_{WCE4}$ experiments were counterbalanced and became weakened compared to those in both MH$_{WC}$ and MH$_{WCE2}$ experiments (contours in Figure 3f, 3i, and 3l).

Hence, the enhanced northward WAM forced by lakes can be explained by lake expansions that induce a cyclonic circulation in the lower atmosphere, accompanied by a weakened AEJ and stronger TEJ associated with weakened Sahara Highs and SHL. Similar mechanisms have been previously identified based on observations and simulations, although their physical mechanisms are still under discussion (Nicholson, 2009; Lavaysse et al., 2010; Klein et al., 2015; Nicholson & Klotter, 2020). Furthermore, we found that the lake-induced precipitation and SM increment were close to those induced by orbital forcing only, but restricted over ~10° N (Figure S4a and S4b). It confirms that lake expansion considerably affected the humidification of NAf. In summary, Western Sahara lake and Megalake Chad could enhance northward WAM triggered by orbital forcings, resulting in a significant humidifying effect.

https://doi.org/10.5194/cp-2023-11
Preprint. Discussion started: 20 March 2023

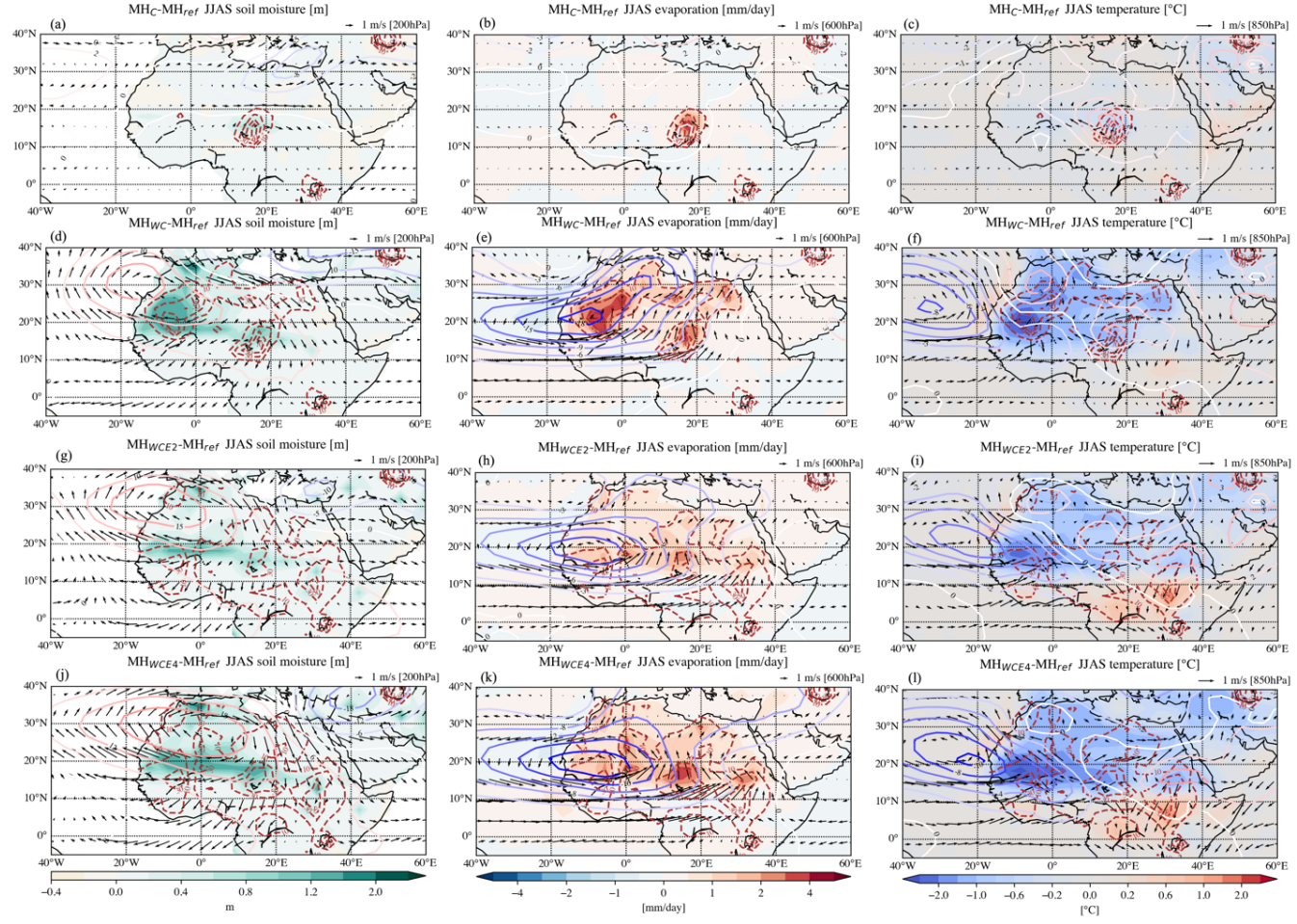

Figure 3: Simulated mid-Holocene climatological JJAS mean anomalies with respect to MH_{ref}: (a) soil moisture (shades) with 200 hPa wind (arrows) and geopotential height (contours), (b) evaporation (shades) with 600 hPa horizontal wind (arrows) and geopotential height (contours) and (c) surface temperature (shades) with 850 hPa horizontal wind (arrows), and geopotential height (contours) for MH_C experiment. Map (d), (g) and (f) are the same as (a), (b) and (c), respectively, but for MH_{WC} experiment. Maps (g), (h) and (i) are the same as (a), (b) and (c), respectively, but for the MH_{WCE2} experiment. Maps (j), (k) and (l) are the same as (a), (b) and (c), respectively, but for the MH_{WCE4} experiments. For all the maps, the lake fraction [%] contours of the respective lake sensitivity experiment are shown with the red dashed lines, and the respective reference scale for the arrow is shown at the right top of each panel.

3.3 Aridity transformation with lake expansions

To understand the influence of Western Sahara lakes and Megalake Chad on the hydroclimatic spatial response, we further calculated the anomaly changes of zonally averaged hydroclimate variables with lake expansion over NAf (Figure 4). Considering PI_{ref} experiments as the reference, the annual mean variables exhibit linear relationships with the mean lake fraction over NAf. Precipitation (Prcp), Evap, and Radiation (Rad) increase with lake fraction, whereas T2 decreases (crosses in Figure 4). However, the unusually higher anomalies in the MH_{WC} experiments suggested that the importance of the lake position potentially outweighs the proportion of lakes. Specifically, the statistical analysis results for summer

https://doi.org/10.5194/cp-2023-11
Preprint. Discussion started: 20 March 2023

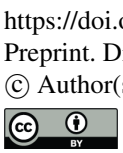

Climate of the Past Discussions
Open Access
EGU

indicate considerable offsets in the MH_{WC} results (positive anomaly offsets for Prcp, Evap, and Rad and negative anomaly offsets for T2; upward triangles in Figure 4), whereas for winter, these variables were not related with the lake expansion (standard deviation = ~0.1), but a cooling effect still existed (downward green triangles in Figure 4). Additionally, lake expansion mainly contributes to the hydrological changes in summer, that is, wetter and cooler conditions are simulated in summer in the lake sensitivity experiments than in the MH_{ref} one.

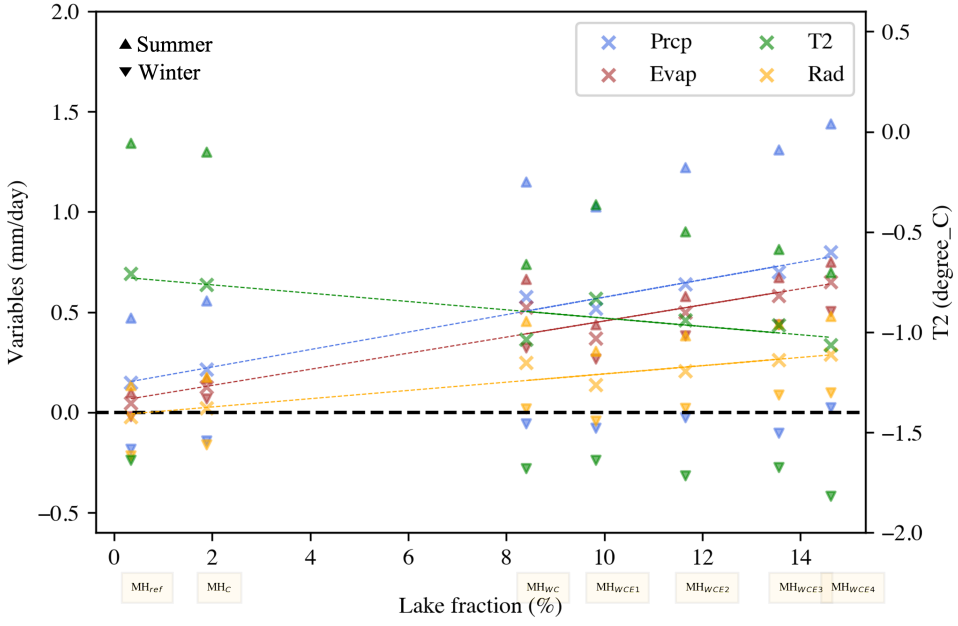

Figure 4: Statistical relationship between averaged zonally hydroclimate variables anomaly and averaged grid lake fraction over Northern Africa (20°W–40E, 0–35°N) for MH lake experiments anomalies (relative to PIref) on the annual (cross), JJAS (upward triangle) and JAM (downward triangle) averages. The hydroclimatic variables include precipitation (Prcp [mm/day]; blue), evaporation (Evap [mm/day]; brown), 2 m air temperature (T2 [°C]; green), and radiation (Rad [mm/day], downward as positive; yellow). The p-value is less than 0.05 for all the relationships.

We used here the Budyko aridity index to detect changes in hydroclimatic conditions related to lake expansion. Compared with the MH_{ref} experiments (Figure S5a), the northwest climate zones are transferred from hyper-arid to arid and semi-arid zones due to the lake expansions in our six MH sensitivity experiments. Moreover, the western arid and semi-arid zone areas are reduced with increasing northward humid and semi-humid zones, along with increasing tropical humid zones (Figure S6). Additionally, in the MH_{WCE4} experiments, such climate zones extend further eastward, corresponding to the spatial response of hydroclimatic variables. Correspondingly, the mean Budyko aridity index anomaly over NAf relative to PI_{ref} increases with lake expansion, indicating that the aridity extent is lower with the presence of lakes (dots in Figure 5a). Climate zone transformation indicates the essential role of lake-climate feedback in sustaining the northwest humidification of the Sahara by changing the hydroclimatic conditions and alleviating aridity.

However, our climate zone results show that there are still hyper-arid and arid zones over the northwestern Sahara. Hence, we further estimated the precipitation scarcity and surplus based on the threshold of semi-humid climate zones ($I \leq 2$),

https://doi.org/10.5194/cp-2023-11
Preprint. Discussion started: 20 March 2023

Climate of the Past Discussions

implying that the climate zones over NAf were at least semi-humid or wetter. The total amount of precipitation scarcity was ~140–160 mm/d, and the precipitation surplus was ~270–380 mm/d over NAf and continued to increase with lake expansion (bars in Figure 5a). Compared with the MH_{ref} results, the MH_{WCE4} experiments potentially reduced precipitation scarcity by up to ~13% and increased precipitation surplus by ~40%. The spatial patterns showed that the north-dry and south-wet modes (Figures S5b and S7) and the dividing line moved up to ~5° to the north compared with the MH_{C} experiments over the western NAf regions (Figure 5b). Additionally, precipitation scarcity was less in the west and more in the east.

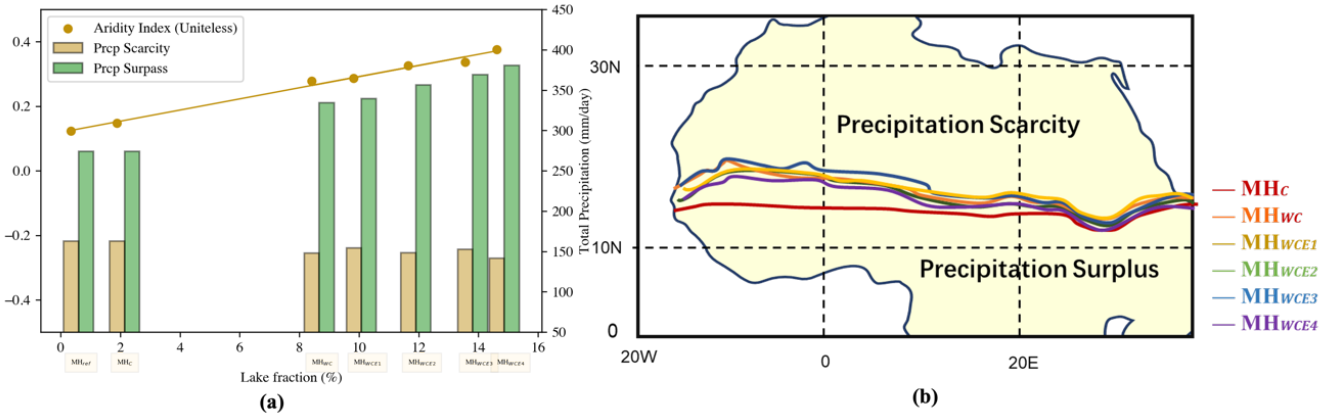

Figure 5: (a) Budyko Aridity index anomaly between PI_{ref} and MH simulations (left y-axis; unitless) with different averaged grid lake fractions as well as the total precipitation scarcity amount (brown bar; mm/day) and total precipitation surplus amount (green bar; mm/day) corresponding to the right y-axis. All the variables are climatological mean annual values. (b) The boarding line between precipitation scarcity zones and precipitation surplus zones for all the mid-Holocene experiments.

Notably, such north-south inverse patterns were also observed in the spatial responses of SM (Figure 3g and 3j), Evap (Figures 3h and 3k), and T2 (Figures 3i and 3l). Specifically, SM and Evap showed positive anomalies with a cooling effect in the north of 10° N, and minor or negative anomalies with a warming effect in the south of 10° N over NAf. However, the enhanced precipitation belt covered the entire tropical area (0°–20° N) in MH_{WCE2} and MH_{WCE4}, and not just the WAM regions (around 10°–20° N) as observed in MH_{WC}. To identify the inverse pattern in MH_{WCE2} and MH_{WCE4}, we analysed the stable oxygen isotope ratio ($\delta^{18}O$) in precipitation (Figure S8), which suggested an oceanic moisture source in addition to the local lakes. Further, the decrease in $\delta^{18}O$ (Figure S8d) with weakened evaporation (Figure 3k) and warming effects (Figure 3l) in the equatorial land areas suggested that the precipitation increment was irrelevant to the westerly monsoon winds. Such an inverse warming effect induced by equatorial lakes may be related to the special equatorial location with lake heating differences during daytime and night (Thiery et al., 2015). Hence, lakes in WAM regions exert wetter and cooler climatic responses. Contrastingly, if lakes are not located in WAM regions, lakes do not affect the northward WAM movement, like the eastern lakes in South Sudan.

https://doi.org/10.5194/cp-2023-11
Preprint. Discussion started: 20 March 2023

Climate of the Past Discussions

4 Discussion and Conclusions

Based on the MIROC5-iso model simulation results using different GS lake maps, we discussed the roles of Western Sahara lakes and Megalake Chad positively influencing the northward movement and eastward expansion of WAM humidifying the Sahara region. Our results showed that Western Sahara lakes promote the northward movement of WAM, and Megalake Chad can further enhance the monsoon westerly flow response eastward. This cyclonic response in the lower atmosphere, associated with weakened AEJ, SHL, Sahara Highs, and strengthened TEJ (Figure 6). Additionally, the humidifying transformation of the climate zone and the reduction in precipitation scarcity over NAf further highlight the important influence of lake expansion in reconstructing the GS climate.

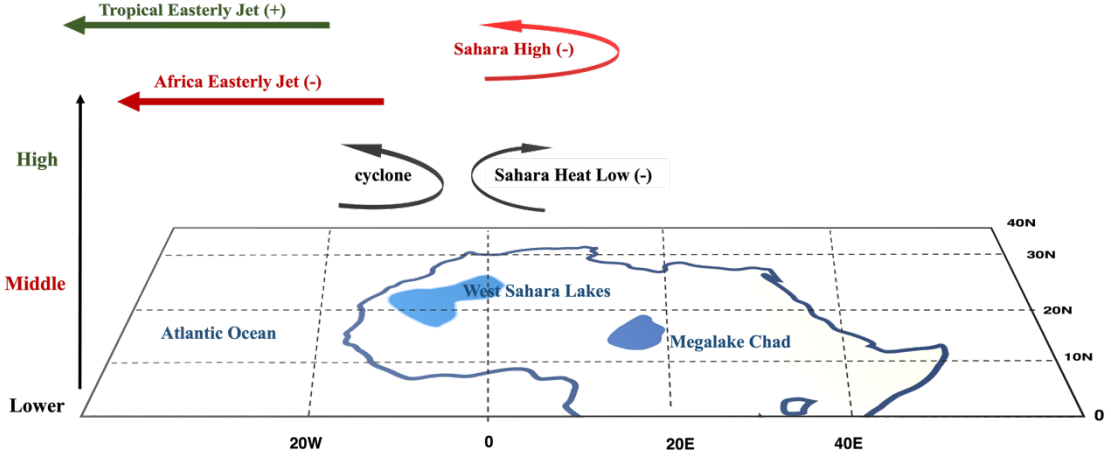

Figure 6: Lake-climate feedback mechanism over North Africa in the mid-Holocene. The lower, middle, and high atmosphere circulation are marked with black, red, and green colors, respectively. The weakening signal is represented by '-', and the strengthening signal is represented by '+'.

Our study confirmed that Megalake Chad does not influence the northward monsoon movement when western lakes are missing (Broström et al., 1998; Carrington et al., 2001; Chandan & Peltier, 2020). We also confirmed the influence of Western Sahara lakes on the northward monsoon movement (Specht et al., 2022), but further stressed that Megalake Chad could extend the westerly monsoon eastward when accompanied by Western Sahara lakes. Chandan and Peltier (2020) underestimated the contribution of lakes by supposing that the weakened SHL induced by the surface cooling effect would reduce precipitation. However, we found that such SHL weakening effect can be offset by the adjacent cyclonic circulation response in the lower atmosphere, which promotes precipitation. Moreover, we found that the northward WAM movement goes with a weakened AEJ and a strengthened TEJ, in agreement with Specht et al. (2022). Therefore, we emphasized the importance of how the climate model represents the AEJ and TEJ behaviors in reproducing the MH climate (Claussen et al., 2017; Bercos-Hickey et al., 2020; Ngoungue et al., 2021). Furthermore, regarding the lake position (Chandan & Peltier, 2020; Specht et al., 2022), we suggest that western lakes and Megalake Chad should be located in the WAM regions to induce the monsoon movement. Finally, the influence of Sahara lakes on climatic zone transformation in NAf is important, as corroborated by the Budyko aridity index. Such lake-climate response can humidify GS by transforming the climate zones

https://doi.org/10.5194/cp-2023-11
Preprint. Discussion started: 20 March 2023

from hyper-arid or arid to semi-arid or semi-humid, especially over the northwestern areas, and reduce the precipitation scarcity by up to 13%.

Limited by the model integration and uncertainty, especially the dynamic lake or vegetation modules coupled with MIROC5-iso, the model-dependent findings of this study only focused on how the changes in the presence of lakes in terms of surface boundary conditions influence the GS hydroclimatic conditions without considering the climate reinforcement on lake expansion or shrinkage. Additionally, under the forcing of lake presence, the soil properties and vegetation growth changes also influence the water holding capacity, which determines the greening process. But these changes are limited by the simplified single-direction feedback discussion. Hence, dynamic model integration is required to provide new insights to understand single variable interactions and their joint effect on land-atmosphere interaction during the GS period (Dallmeyer et al., 2020). Moreover, understanding the outer components, such as orbital forcing and greenhouses, which influence the GS climate system, would also provide insights into replicating the GS climate in the future (Duque-Villegas et al., 2022). Thus far, the interactive dynamic understanding among potential GS climate drivers is still unclear and different types of interactive feedback mechanisms contributing to the limitation of the uncertainty should be identified through climate proxy datasets.

In summary, our study identified lake expansions during the MH that sustain the Sahara greening with a northward movement and eastward extension of WAM. Limited by model dependency and module integration, the land-atmosphere interaction mechanism forced by dynamic lake changes remains unclear. In the future, the dynamic lake module will be improved to detect the lake-climate interaction with time-varying lake extent in the simulations. Such research will reveal the dynamic interactive mechanism of lake-climate interactions and the possible conditions sustaining the Sahara greening processes

https://doi.org/10.5194/cp-2023-11
Preprint. Discussion started: 20 March 2023

Code Availability

The code of the isotopic version MIROC5-iso is available upon request on the IIS's GitLab repository http://isotope.iis.u-tokyo.ac.jp:8000/gitlab/miroc-iso/miroc5-iso (Okazaki and Yoshimura, 2019).

Data Availability

The paleo small lake reconstruction maps (Hoelzmann, Jolly et al., 1998) and potential maximum lake reconstruction maps (Tegen, Harrison et al., 2002) used in this study for comparison are the processed ones published by Specht, Claussen et al. (2022), available at http://hdl.handle.net/21.11116/0000-0009-63B5-B. The updated 15 arc-second lake maps over the NA (Chen, Ciais et al., 2021) are available at Mendeley Data http://dx.doi.org/10.17632/8vfhhv8s2f.1 and we used the RFM2 model results in this study. Isotopic proxy datasets from ice cores used for the climate model validation method are reported in Table 1 Cauquoin et al. (2019). The SISALv2 dataset is available at https://doi.org/10.17864/1947.256 (Comas-Bru, Rehfeld et al. 2020).

Author contributions

KK and OT designed the research idea. YL and KK contributed to the experiment design. KK and AC provided model code and input data. YL performed the model experiments and results analysis. YL prepared the manuscript with contributions from all co-authors.

Competing interests.

The authors have no other competing interests to declare.

Acknowledgments

This work was supported by the Japan Society for the Promotion of Science [KAKENHI; 21H05002], the Environment Research and Technology Development Fund (JPMEERF20202005) of the Environmental Restoration and Conservation Agency of Japan, the Japan Society for the Promotion of Science via Grants-in-Aid 22K21323 and the advanced studies of climate change projection (SENTAN; JPMXD0722680395) from the Ministry of Education, Culture, Sports, Science and Technology (MEXT), Japan.

https://doi.org/10.5194/cp-2023-11
Preprint. Discussion started: 20 March 2023

References

Bercos-Hickey, E., Nathan, T. R., & Chen, S.-H. (2020). On the Relationship between the African Easterly Jet, Saharan Mineral Dust Aerosols, and West African Precipitation. Journal of Climate, 33(9), 3533-3546. doi:10.1175/jcli-d-18-0661.1

Berger, A. (1988). Milankovitch Theory and climate. 26(4), 624-657. doi:https://doi.org/10.1029/RG026i004p00624

Biasutti, M., & Sobel, A. H. (2009). Delayed Sahel rainfall and global seasonal cycle in a warmer climate. Geophysical Research Letters, 36(23). doi:10.1029/2009gl041303

Braconnot, P., Albani, S., Balkanski, Y., Cozic, A., Kageyama, M., Sima, A., . . . Peterschmitt, J.-Y. (2021). Impact of dust in PMIP-CMIP6 mid-Holocene simulations with the IPSL model. Climate of the Past, 17(3), 1091-1117. doi:10.5194/cp-17-1091-2021

Braconnot, P., Otto-Bliesner, B., Harrison, S., Joussaume, S., Peterchmitt, J. Y., Abe-Ouchi, A., . . . Zhao, Y. (2007). Results of PMIP2 coupled simulations of the Mid-Holocene and Last Glacial Maximum – Part 1: experiments and large-scale features. Clim. Past, 3(2), 261-277. doi:10.5194/cp-3-261-2007

Brierley, C. M., Zhao, A., Harrison, S. P., Braconnot, P., Williams, C. J. R., Thornalley, D. J. R., . . . Abe-Ouchi, A. (2020). Large-scale features and evaluation of the PMIP4-CMIP6 <i>midHolocene</i> simulations. Climate of the Past, 16(5), 1847-1872. doi:10.5194/cp-16-1847-2020

Broström, A., Coe, M., Harrison, S. P., Gallimore, R., Kutzbach, J. E., Foley, J., . . . Behling, P. (1998). Land surface feedbacks and palaeomonsoons in northern Africa. Geophysical Research Letters, 25(19), 3615-3618. doi:10.1029/98gl02804

Budyko, M. I., & Miller, D. H. (1974). Climate and Life: Academic Press.

Carrington, D. P., Gallimore, R. G., & Kutzbach, J. E. (2001). Climate sensitivity to wetlands and wetland vegetation in mid-Holocene North Africa. Climate Dynamics, 17(2-3), 151-157. doi:https://doi.org/10.1007/s003820000099

Cauquoin, A., Werner, M., & Lohmann, G. (2019). Water isotopes – climate relationships for the mid-Holocene and preindustrial period simulated with an isotope-enabled version of MPI-ESM. Climate of the Past, 15(6), 1913-1937. doi:10.5194/cp-15-1913-2019

Chandan, D., & Peltier, W. R. (2020). African Humid Period Precipitation Sustained by Robust Vegetation, Soil, and Lake Feedbacks. Geophysical Research Letters, 47(21). doi:10.1029/2020gl088728

Cheddadi, R., Carre, M., Nourelbait, M., Francois, L., Rhoujjati, A., Manay, R., . . . Schefuss, E. (2021). Early Holocene greening of the Sahara requires Mediterranean winter rainfall. Proc Natl Acad Sci U S A, 118(23). doi:10.1073/pnas.2024898118

Chen, W., Ciais, P., Qiu, C., Ducharne, A., Zhu, D., Peng, S., . . . Huang, C. (2021). Wetlands of North Africa During the Mid-Holocene Were at Least Five Times the Area Today. Geophysical Research Letters, 48(20). doi:10.1029/2021gl094194

Chen, W., Ciais, P., Zhu, D., Ducharne, A., Viovy, N., Qiu, C., & Huang, C. (2020). Feedbacks of soil properties on vegetation during the Green Sahara period. Quaternary Science Reviews, 240. doi:10.1016/j.quascirev.2020.106389

https://doi.org/10.5194/cp-2023-11
Preprint. Discussion started: 20 March 2023

Claussen, M., Dallmeyer, A., & Bader, J. (2017). Theory and Modeling of the African Humid Period and the Green Sahara. In: Oxford University Press.

Comas-Bru, L., Harrison, S. P., Werner, M., Rehfeld, K., Scroxton, N., Veiga-Pires, C., & members, S. w. g. (2019). Evaluating model outputs using integrated global speleothem records of climate change since the last glacial. Clim. Past, 15(4), 1557-1579. doi:10.5194/cp-15-1557-2019

Comas-Bru, L., et al. (2020). "SISALv2: a comprehensive speleothem isotope database with multiple age–depth models." Earth Syst. Sci. Data 12(4): 2579-2606.

Dallmeyer, A., Claussen, M., Lorenz, S. J., & Shanahan, T. (2020). The end of the African humid period as seen by a transient comprehensive Earth system model simulation of the last 8000 years. Climate of the Past, 16(1), 117-140. doi:10.5194/cp-16-117-2020

Duque-Villegas, M., Claussen, M., Brovkin, V., & Kleinen, T. (2022). Effects of orbital forcing, greenhouse gases and ice sheets on Saharan greening in past and future multi-millennia. Climate of the Past, 18(8), 1897-1914. doi:10.5194/cp-18-1897-2022

Fudge, T. J., Steig, E. J., Markle, B. R., Schoenemann, S. W., Ding, Q., Taylor, K. C., . . . Members, W. D. P. (2013). Onset of deglacial warming in West Antarctica driven by local orbital forcing. Nature, 500(7463), 440-444. doi:10.1038/nature12376

Harrison, S. P., Bartlein, P. J., Izumi, K., Li, G., Annan, J., Hargreaves, J., . . . Kageyama, M. (2015). Evaluation of CMIP5 palaeo-simulations to improve climate projections. Nature Climate Change, 5(8), 735-743. doi:10.1038/nclimate2649

Hoelzmann, P., Jolly, D., Harrison, S. P., Laarif, F., Bonnefille, R., & Pachur, H. J. (1998). Mid-Holocene land-surface conditions in northern Africa and the Arabian Peninsula: A data set for the analysis of biogeophysical feedbacks in the climate system. Global Biogeochemical Cycles, 12(1), 35-51. doi:10.1029/97gb02733

Holmes, J., & Hoelzmann, P. (2017). The late pleistocene-holocene African humid period as evident in lakes. In Oxford Research Encyclopedia of Climate Science.

Hopcroft, P. O., & Valdes, P. J. (2019). On the Role of Dust-Climate Feedbacks During the Mid-Holocene. Geophysical Research Letters, 46(3), 1612-1621. doi:10.1029/2018gl080483

Kino, K., Okazaki, A., Cauquoin, A., & Yoshimura, K. (2021). Contribution of the Southern Annular Mode to Variations in Water Isotopes of Daily Precipitation at Dome Fuji, East Antarctica. Journal of Geophysical Research: Atmospheres, 126(23). doi:10.1029/2021jd035397

Klein, C., Heinzeller, D., Bliefernicht, J., & Kunstmann, H. (2015). Variability of West African monsoon patterns generated by a WRF multi-physics ensemble. Climate Dynamics, 45(9-10), 2733-2755. doi:10.1007/s00382-015-2505-5

Krinner, G., Lézine, A. M., Braconnot, P., Sepulchre, P., Ramstein, G., Grenier, C., & Gouttevin, I. (2012). A reassessment of lake and wetland feedbacks on the North African Holocene climate. Geophysical Research Letters, 39(7). doi:https://doi.org/10.1029/2012GL050992

Kuete, G., Mba, W. P., James, R., Dyer, E., Annor, T., & Washington, R. (2022). How do coupled models represent the African Easterly Jets and their associated dynamics over Central Africa during the September–November rainy season? Climate Dynamics. doi:10.1007/s00382-022-06467-y

Kutzbach, J., Bonan, G., Foley, J., & Harrison, S. P. (1996). Vegetation and soil feedbacks on the response of the African monsoon to orbital forcing in the early to middle Holocene. Nature, 384(6610), 623-626. doi:10.1038/384623a0

Kutzbach, J. E., Guan, J., He, F., Cohen, A. S., Orland, I. J., & Chen, G. (2020). African climate response to orbital and glacial forcing in 140,000-y simulation with implications for early modern human environments. Proc Natl Acad Sci U S A, 117(5), 2255-2264. doi:10.1073/pnas.1917673117

Lavaysse, C., Flamant, C., & Janicot, S. (2010). Regional-scale convection patterns during strong and weak phases of the Saharan heat low. Atmospheric Science Letters, 11(4), 255-264. doi:10.1002/asl.284

Messori, G., Gaetani, M., Zhang, Q., Zhang, Q., & Pausata, F. S. R. (2018). The water cycle of the mid-Holocene West African monsoon: The role of vegetation and dust emission changes. International Journal of Climatology, 39(4), 1927-1939. doi:10.1002/joc.5924

Ngoungue Langue, C. G., Lavaysse, C., Vrac, M., Peyrillé, P., & Flamant, C. (2021). Seasonal forecasts of the Saharan heat low characteristics: a multi-model assessment. Weather and Climate Dynamics, 2(3), 893-912. doi:10.5194/wcd-2-893-2021

Nicholson, S. E. (2009). On the factors modulating the intensity of the tropical rainbelt over West Africa. International Journal of Climatology, 29(5), 673-689. doi:10.1002/joc.1702

Nicholson, S. E., & Klotter, D. (2020). The Tropical Easterly Jet over Africa, its representation in six reanalysis products, and its association with Sahel rainfall. International Journal of Climatology, 41(1), 328-347. doi:10.1002/joc.6623

O'Ishi, R., & Abe-Ouchi, A. (2011). Polar amplification in the mid-Holocene derived from dynamical vegetation change with a GCM. Geophysical Research Letters, 38(14), n/a-n/a. doi:10.1029/2011gl048001

Ohgaito, R., Yamamoto, A., Hajima, T., O'Ishi, R., Abe, M., Tatebe, H., . . . Kawamiya, M. (2021). PMIP4 experiments using MIROC-ES2L Earth system model. Geoscientific Model Development, 14(2), 1195-1217. doi:10.5194/gmd-14-1195-2021

Okazaki, A., & Yoshimura, K. (2019). Global Evaluation of Proxy System Models for Stable Water Isotopes With Realistic Atmospheric Forcing. Journal of Geophysical Research: Atmospheres, 124(16), 8972-8993. doi:10.1029/2018jd029463

Otto-Bliesner, B. L., Braconnot, P., Harrison, S. P., Lunt, D. J., Abe-Ouchi, A., Albani, S., . . . Zhang, Q. (2017). The PMIP4 contribution to CMIP6 – Part 2: Two interglacials, scientific objective and experimental design for Holocene and Last Interglacial simulations. Geoscientific Model Development, 10(11), 3979-4003. doi:10.5194/gmd-10-3979-2017

Perez-Sanz, A., Li, G., González-Sampériz, P., & Harrison, S. P. (2014). Evaluation of modern and mid-Holocene seasonal precipitation of the Mediterranean and northern Africa in the CMIP5 simulations. Climate of the Past, 10(2), 551-568. doi:10.5194/cp-10-551-2014

Quade, J., Dente, E., Armon, M., Ben Dor, Y., Morin, E., Adam, O., & Enzel, Y. (2018). Megalakes in the Sahara? A Review. Quaternary Research, 90(2), 253-275. doi:10.1017/qua.2018.46

455 Risi, C., Bony, S., Vimeux, F., & Jouzel, J. (2010). Water-stable isotopes in the LMDZ4 general circulation model: Model evaluation for present-day and past climates and applications to climatic interpretations of tropical isotopic records. 115(D12). doi:https://doi.org/10.1029/2009JD013255

Specht, N. F., Claussen, M., & Kleinen, T. (2022). Simulated range of mid-Holocene precipitation changes from extended lakes and wetlands over North Africa. Climate of the Past, 18(5), 1035-1046. doi:10.5194/cp-18-1035-2022

460 Sturm, C., Zhang, Q., & Noone, D. (2010). An introduction to stable water isotopes in climate models: benefits of forward proxy modelling for paleoclimatology. Clim. Past, 6(1), 115-129. doi:10.5194/cp-6-115-2010

Sundqvist, H. S., Kaufman, D. S., McKay, N. P., Balascio, N. L., Briner, J. P., Cwynar, L. C., . . . Viau, A. E. (2014). Arctic Holocene proxy climate database – new approaches to assessing geochronological accuracy and encoding climate variables. Clim. Past, 10(4), 1605-1631. doi:10.5194/cp-10-1605-2014

465 Tegen, I., Harrison, S. P., Kohfeld, K., Prentice, I. C., Coe, M., & Heimann, M. (2002). Impact of vegetation and preferential source areas on global dust aerosol: Results from a model study. Journal of Geophysical Research: Atmospheres, 107(D21), AAC 14-11-AAC 14-27. doi:10.1029/2001jd000963

Thiery, W., Davin, E. L., Panitz, H.-J., Demuzere, M., Lhermitte, S., & van Lipzig, N. (2015). The Impact of the African Great Lakes on the Regional Climate. Journal of Climate, 28(10), 4061-4085. doi:10.1175/jcli-d-14-00565.1

470 Thompson, A. J., Zhu, J., Poulsen, C. J., Tierney, J. E., & Skinner, C. B. (2022). Northern Hemisphere vegetation change drives a Holocene thermal maximum. Sci Adv, 8(15), eabj6535. doi:10.1126/sciadv.abj6535

Thorncroft, C. D., Nguyen, H., Zhang, C., & Peyrillé, P. (2011). Annual cycle of the West African monsoon: regional circulations and associated water vapour transport. Quarterly Journal of the Royal Meteorological Society, 137(654), 129-147. doi:10.1002/qj.728

475 Tootchi, A., Jost, A., & Ducharne, A. (2019). Multi-source global wetland maps combining surface water imagery and groundwater constraints. Earth System Science Data, 11(1), 189-220. doi:10.5194/essd-11-189-2019

Watanabe, M., Suzuki, T., O'ishi, R., Komuro, Y., Watanabe, S., Emori, S., . . . Kimoto, M. (2010). Improved Climate Simulation by MIROC5: Mean States, Variability, and Climate Sensitivity. Journal of Climate, 23(23), 6312-6335. doi:10.1175/2010jcli3679.1

480